Computer-Assisted Design of hydroxamic acid derivatives Inhibitors of M1 metallo aminopeptidase of*Plasmodium falciparum*with Favorable Pharmacokinetic Profile

Abstract

We virtually design here new subnanomolar range antimalarial, inhibitors of *plasmodium falciparum* M1 Aminopeptidase (*Pf*A-M1), by means of structure-based molecular design. We developed the complexation QSAR models from Hydroxamic Acid derivatives (AHO). A linear correlation was established between the computed Gibbs free energies of binding (GFE: $\Delta\Delta G_{com}$) and observed enzyme inhibition constants (K_i^{exp}) for each training set $pK_i^{exp} = -0.063\times\Delta\Delta G_{com} + 8.003$, $R^2 = 0.92$. The predictive power of the QSAR model was validated with 3D-QSAR pharmacophore generation (PH4): $pK_i^{exp} = 1.0289\times pK_i^{pred} - 0.155$, $R^2 = 0.90$. We then conducted a study on catalytic residues to exploit the different interactions (enzyme: inhibitor). Structural information from the models guided us in designing of a virtual combinatorial library (VCL) of more than 44 thousands AHOs. The PH4 screening retained 51 new and potent AHOs with predicted inhibitory potencies pK_i^{pre} up to 13 times lower than that of AHO1 (pK_i^{exp} = 700 nM). Combining molecular modeling and PH4 in silico screening of the VCL resulted in the proposed novel potent antimalarial agent candidates with favorable pharmacokinetic profiles.

KEYWORDS

Drug Design, QSAR Model, Pharmacophore Model, Complexation Model, Molecular Modelling, ADMET

Introduction

Malaria is an endemic disease caused by parasiticprotozoans of the genus *Plasmodium*, the most defeating being *Plasmodium falciparum* (*Pf*) with a widegeographical distribution. The parasite dormant liver stage able to reactivate after months without reinfection greatens the burden of malaria.The bewildering 2020 burden of "an estimated 241 million malaria cases and 627 000 deaths (77% are children aged under 5 years) in 85 malaria endemic countries (including the territory of French Guiana), despite the Covid-19 pandemic disruption of service 2020,namely 59‰ cases and 15.3‰ deaths (‰: for 1000 population at risk) is an increase in comparison to WHO 2019 annual report [1,2]. According to the same 2020 report 37% of R&D funding went to drugs, 28% to basic research, 19% to vaccine, 10% to vector control products and the remaining to diagnostics, biologicals, etc. revealing marginal changes from 2019 such as a decrease of 1.6% for drugs and an increase of 1.6% for basic research. The decrease of vaccine funding has to be separated from its increase for early-stage malaria [1]. The top position of drugs and basic research outweigh the emergence and spread of artemisinin-resistant*Plasmodium falciparum*in WHO African region (East Africa) after the Cambodia and Thailand Mekong subregion [1, 3, 4, 5] considered as the unfacing disasterthat the WHO early 2000s ACTs strategy is designed to avoid with the mandatory expectation that in the meantime (almost two decades) an alternative artemisinin-equipotent drug will be discovered. When is this crucial new drug to tackle definitely the ingenuity of *Plasmodium falciparum*expected toreach market?During the last stage of hemoglobin degradation aminopeptidase cleave the dipeptides and oligopeptides to their constituent amino acids [6,7]. They are metal ion-containing exopeptidases where the metal ion acts as enzyme-catalyzed reaction promotor by favoring hydrolysis [8, 9]. Among the nine *Plasmodium falciparum*identified metallo-aminopeptidases (MAPs),the neutral M1 alanyl-aminopeptidase (*Pf*A-M1) and M17 Leucyl aminopeptidase (*Pf*A-M17) are the most studied and validated as essential *Pf* enzyme targets whose inhibition should be lethal [10,11] making them attractive for the design of a new class of antimalarials [12].Their expression at various stages of the *Plasmodium* life cycle increases its interest and druggability [12,13]. Various scaffolds have been designed as inhibitors of *Pf*A-M1 including the natural product Bestatin (1)mimicking the dipeptide D-Phe-L-Leu with the hydroxyl containing zinc ion binding group in red and the Phe (benzyl) and Leu (isoleucine) moieties fitting in the S1 (phenyl ring in π---π contact with Tyr575) and S1' pockets respectivelyreaching a biological activity of 190 nM [14]. A para-methoxy substitution on the P1 benzyl to fill better the S1 pocket results in a fourfold potency increase (K_i = 43 nM) indicating that S1 pocket can accommodate bulkier group [14]. Phosphinates dipeptide (2) are dual-targets inhibitors of both *Pf*A-M1 and *Pf*A-M17binding to *Pf*A-M1 through a bivalent contact with the zinc ion while the P1 (S1 pocket) and P1' (S1' pocket) phenyls are in π---π contact with Tyr575 and the catalytic His496 respectively [15].Phosphonatesinhibitors (3), (4),also are dual targets design to fit specifically the large S1 pocket of *Pf*A-M1 the phosphate group interacting with the zinc ion with the most potent (3) reaching 11 μM,the hydrophobic contact of4-(1H-pyrazol-1-yl) phenyl group filling the *Pf*A-M1 S1 pocket (K_i = 104 μM)did not increase the binding affinity as thatwas for *Pf*A-M17 (K_i = 11 nM) [16]. Hydroxamate is well known orally safe drug design zinc binding group[17] and malonic hydroxamate inhibitors exemplified by (5)in the rigidified phenylmeth-(Z/E)-ylidenegeometry have high activity against *Pf*A-M1 (IC_{50} = 6 nM); thisis explained by the Z-isomer instead of the E-isomer from docking experiment.The non-rigidifiedinhibitor is almost fivefold less potent (IC_{50} = 27 nM); the benzylmalonyl group fits into the

S1’ pocket and the phenylmeth-(Z)-ylidenemoeity seats in the hydrophobic S1 [18]. More recently amino-hydroxamic acid has emerged in place of phosphonates due to their better pharmacokinetic profile as common drug design zinc ion binding groupcombined with the promising 4-(1H-pyrazol-1-yl) phenyl in P1 and a pivaloyl group in P1’increasing the activity K_i from 107 (4) to 0.7 μM for N-(1-(4-(1H-Pyrazol-1-yl) phenyl)-2-(hydroxyamino)-2-oxoethyl)- pivalamide (6)[17, 19]. Replacement of 4-(1H-pyrazol-1-yl) phenyl in P1 by para bromophenyl (7) resulted in a surprising raise of potency to K_i = 27 nM [20]. The same authors reported a K_i = 78 nM with a 3,4,5-trifluorophenyl in place of p-Ph moiety in P1 and tButyl in P1’ (8); and they reconsidered that potency in a subsequent paper with altered methodology to a K_i of 331 nM [21]. Keeping in (8) the trifluorophenyl and enlarging the tertiary-butylcarbonyl to a tertiary-butyloxycarbonyl moiety is detrimental to activity (9): K_i = 19 000 nM. All this suggests a lack of evidence about suitable pharmacophore of *Pf*A-M1 active site to guide straightforward selection of R-groups in order to fill S1 and S1’ pockets advantageously. Accordingly we retain in our study the better and safer zinc ion binding group (R_2: hydroxamate) along with R_3–phenyl in P1 and varying P1’ substitution groups (R_1)as SAR [19]from which a complexation QSAR model (10)will be built as well as a subsequent 3D-QSAR pharmacophore model as navigator to virtually explore the hydroxamateanalogs chemical subspace with the expectation of improving binding affinity.

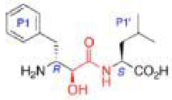

(1)

K_i = **190** nM[14]

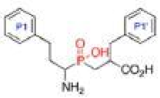

(2)

K_i = **78.4** nM[15]

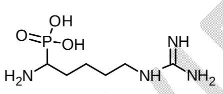

(3)

K_i = **11** μM[16]

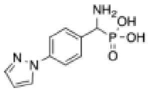

(4)

K_i = **104** μM[16]

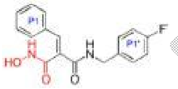

(5)

IC_{50} = **6** nM[18]

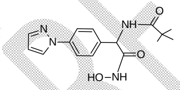

(6)

K_i = **700** nM[19]

(7)

K_i = **27** nM[20]

(8)

K_i = **78** nM[20]
K_i = **331** nM[21]

(9)

K_i = **19000** nM[20]

(10)

Figure 1: Inhibitors of *Pf*A-M1.

The metrics describing interactions at the *Pf*A-M1 active site have been assessed from the X-rays crystal structure analysis of *Pf*A-M1 (PDB code 4R5V) in complex with one of the most active studied inhibitors in this work (6) [19].The zinc ion coordinates the catalytic triad His496, His500, and Glu519 (not displayed on the Fig 2 2D diagram)and the hydroxamate in a network of HB contacts with Glu463, Glu497, His500, His496and Tyr580. The *tert*-butyl moiety hydrophobic contacts in S1’ involve Thr492, Val493 the deepest residue at the pocket baseand Val523.The hydrophobic S1 cavity (Gln317, Val459, Met462, Glu572, Tyr575and Met1034) accommodates the 4-(1H-pyrazol-1-yl) phenyl moiety in π---π stacking with Tyr575, π---alkyl with Val459 and Met1034, and π---sulfur with Met462.

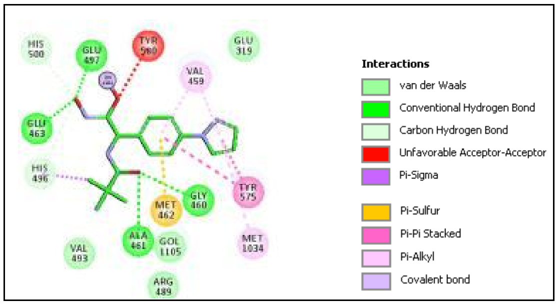

Figure 2: *Pf*A-M1–(6) interactions at active site depicted in 2D.

Methods

General workflow

The general workflow start from SAR results along with the availability of X-ray structure of the target enzyme in complex with either one of the SAR compounds or at least any ligand. From this,*in situ* modification will be performed to carefully build as many complexes as SAR compounds available in the training set. The computation of the Gibbs free energy ($\Delta\Delta G_{com}$) of each complex formation will lead, through a correlation with experimental activity (K_i), to the inhibitors' active conformations. The 3D-QSAR pharmacophore (PH4) generated from the active conformation (correlating AHO training set estimated K_i with experimental ones) will serve to screen a virtual library of AHO analogs to yield a handful of AHO best PH4 fit hits.

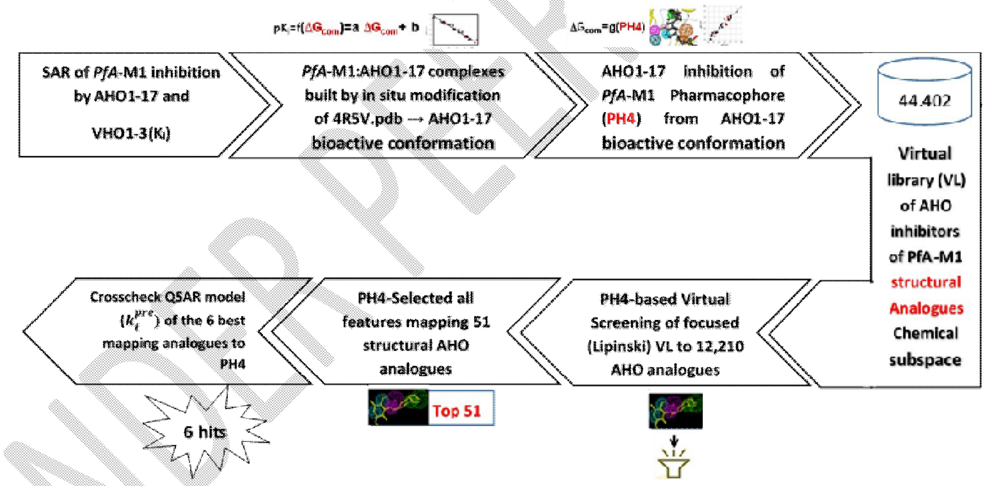

Scheme 1: General workflow of computer assisted AHO analogs design.

Training and Validation Sets

The chemical structures and biological activities (K_i^{exp}) of all the inhibitors used throughout this work are taken from the literature [19,20,21]. TheirK_i^{exp}cover a very wide range ($501{,}500 \geq K_i^{exp} \geq 27$ nM)spanning more than four orders of magnitude,far beyond the threshold of 3.5 suitable for a reliable 3D QSARpharmacophore model [22]. Out of a total of 20 compounds, 17 were used for the training set (TS) and 3 for the validation (VS) set not used to build the QSAR model.

Model Building

The enzymestructure preparation stage is a very important step in the completion of a complexation job. Therefore, molecular models of free inhibitors and complexes have been prepared from high-resolution crystallographic structure using the Insight-II 2005 Molecular Modelling programmeand Discovery Studio Suite [23,24]. The *Pf*A-M1 has 3 crystallographic structures, coded as 4R5X, 4R5T and 4R5V [19] deposited in the Protein Data Bank (PDB) [25]. For this work, we chose the structure coded 4R5V because it crystallizes in a single chain, unlike the others; N-(1-(4-(1H-Pyrazol-1-yl)phenyl)-2-(hydroxyamino)-2-oxoethyl)-pivalamide(AHO3) is the endogenous ligand at the enzyme active site. The structure has been prepared andall crystallographic water moleculeswere removed, then hydrogens were added to the residues of the *Pf*A-M1 and *Pf*A-M1:AHO complex with the protonation/ionization state corresponding to the pH of 7 keeping the N- and C-terminal groups neutral.From this starting structure *in situ* modification of the reference ligand to build all the training set *Pf*A-M1–AHOx complexes through substitutions at R1, R2 and R3positions. Inhibitors were modelled from the 4R5V reference crystal structure by in situ modification of functional groups in the molecular scaffold of the endogenous AHO3 inhibitor. All rotatable bonds of the replacing fragments were subjected to an exhaustive conformational search coupled with a careful gradual energy-minimization of the modified inhibitor and active-site residues of *Pf*A-M1 located in the immediate vicinity (5 Å radius) in order to identify low-energy bound conformations of the modified inhibitors. The resulting low-energy structures of the E:I complexes were then carefully refined by energy-minimization procedure of the entire complex to obtain stable structures of the binary *Pf*A-M1:AHO complexes.The complete description of the computation of relative ligand binding affinity ($\Delta\Delta G_{com}$) has been reported earlier [26].

Molecular Mechanics

The main advantage of molecular mechanics compared to other methods is the speed of the calculations. This is due to a simplification of the force field equations; it is therefore possible to process very large molecular systems. On the other hand, this method does not take into account the molecular electronic structure [27].“However, this study was carried out using the CFF force field” [28].“A dielectric constant of 4 was used for all MM calculations in order to take into account the dielectric shielding effect in proteins. Minimizations of the E:I complexes, free E and I were carried out by relaxing the structures gradually, starting with added hydrogen atoms, continued with residue side chain heavy atoms and followed by the protein backbone relaxation. Geometry optimizations were performed using the sufficient number of steepest descent and conjugate gradient iterative cycles and average gradient convergence criterion of 0.01 kcal.mol^{-1}.Å^{-1}. The process has been described fully earlier” [26].

Conformational Search

Conformational research is a method for calculating the relative energy associated with the conformation of a molecule [29]. Its aim is therefore to find the minimum possible and to calculate Boltzmann's population, which gives us information on the population of occupied levels at a given temperature [30]. To this end, all the free inhibitors used in this study are derived from their conformation linked in E-I complexes.The process has been described fully earlier [31].

Solvation Gibbs Free Energies

“Ligand-receptor interactions take place in a solvent, which contributes through hydrogen bonding and solvation phenomena to the binding process. Theelectrostatic component of the solvation GFE, which includes also the effect of ionic strength of the solvent by solving the nonlinear Poisson–Boltzmann equation [32,33] was computed by the DelPhi module of the Discovery Studio (DS 2.5)” [24]. “The program represents the solvent by a continuous medium of high dielectric constant (ε_{ro}= 80) and the solute as a charge distribution filling a low dielectric cavity (ε_{ri}= 4) with boundaries linked to the solute’s molecular surface. The program numerically solves for the molecular electrostatic potential and reaction field around the solute using finite difference method. DelPhi calculations were done on a (235 × 235 × 235) cubic lattice grid for the E:I complexes and free E and on a (65 × 65× 65) grid for the free I. Full coulombic boundary conditions were employed. Two subsequent focusingsteps led to a similar final resolution of about 0.3 Å per grid unit at 70% filling of the grid by the solute. Physiological ionic strength of 0.145 mol.dm^{-3} , atomic partial charges and radii defined in the CFF force field parameter set

30 and a probe sphere radius of 1.4 Å were used. The electrostatic component of the Poisson–Boltzmann solvation GFE was calculated as the reaction field energy" [34-35].

Calculation of Binding Affinity and QSAR Model

The calculation of binding affinity expressed as complexation GFE has been described fully earlier [26].

Interaction Energy

The force field CFF was used to calculate the interaction energy (E_{int}) between the enzyme residues and the inhibitor as described earlier [26].

Pharmacophore Generation

Discovery Studio[24] through its algorithm program Catalyst HypoGen [36] allowed us to establish the inhibitor conformations from models of different E-I complexes used for the construction of a 3D-QSAR (PH4) pharmacophore.

ADME Properties

The pharmacokinetic profile of AOHs was calculated by the program QikProp [37]as described earlier [26].

Virtual Library (VL) Generation

The virtual library generation was performed as described earlier [26].

ADME-Based Virtual Library focusing

The orientation of the virtual library has been made thanks to numerous selection criteria as described above [**Error! Bookmark not defined.**]. Twenty-four pharmacokinetics-related molecular descriptors available in QikProp [33], which characterize a wide spectrum of molecular properties as described in the footnote of table 7, were used. Optimum ranges of these 24 descriptors were defined in terms of upper and lower bounds according to QikProp [33]. Among them predicted drug-likeness (#stars, footnote of table 7) was used to retain drug-like AHOanalogs in the focused VL.

Pharmacophore-Based Library Searching

The pharmacophore-based virtual library searching was performed as described earlier [26].

Inhibitory Potency Prediction

The conformer with the best mapping on the PH4 pharmacophore in each cluster of the focused library subset was selected for in silico screening by the complexation QSAR model. The computed $\Delta\Delta G_{com}$ of each selected new analog was used for prediction *Pf*A-M17 inhibitory potency (K_i^{pre}) of the focused virtual library of AHO analog by inserting this parameter into the target-specific scoring function given in equation (1) parameterized using the complexation QSAR model of the training set of AHO inhibitors [19,20,21].

$$pK_i^{pre} = -\log_{10} K_i^{pre} = a.\ \Delta\Delta G_{com} + b \qquad (1)$$

RESULTS

Training and Validation Sets

"The training set of 17 AHOs and validation set of another 3 analogs (Table 1) were selected from a homogeneous series of *Pf*A-M1 inhibitors with known experimentally determined inhibitory activities originating from a single laboratory" [19-21]. The whole series was obtained by variations at two positions R2 and R3 on the backbone of hydroxamic acid as show in Table 1. "The experimental biological activities ($27 \leq K_i^{exp} \leq 501500$ nM) [19,20,21] cover a sufficiently wide concentration range for building of a reliable QSAR model. The ratio between the sizes of training and validation sets remains a critical point of correct classification but is limited by the count of the set of homologous compounds available from the literature" [38].

Table 1.Trainingset (AHO1-17) and validation set (VHO1-3) of *Pf*A-M1 inhibitors [19,20,21] used in the preparation of QSAR models of inhibitor binding. The R1, R2 and R3 groups are numbered in the first part of the Table as #R ≡ group index.

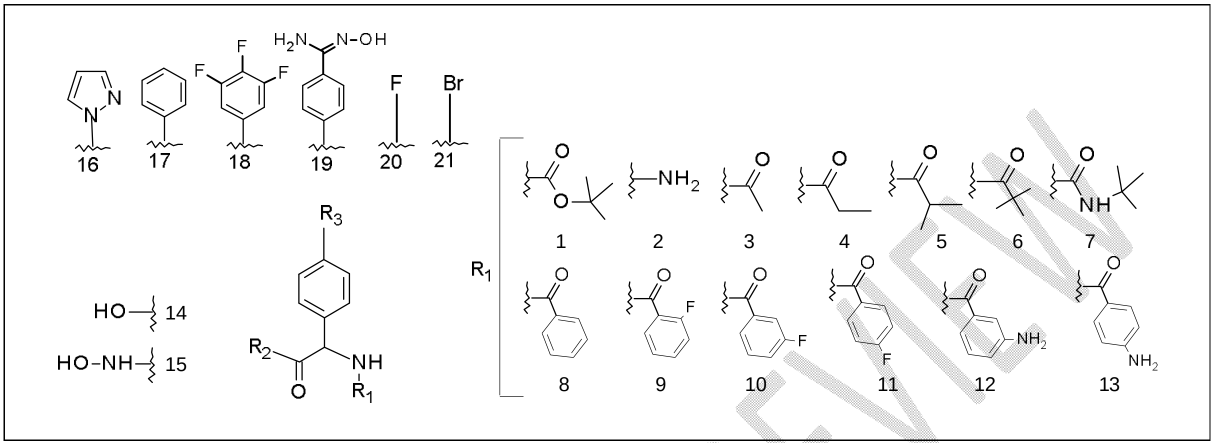

Training set	AHO1	AHO2	AHO3**	AHO4**	AHO5	AHO6	AHO7	AHO8	AHO9	AHO10	AHO11
$\#R_1–\#R_2–\#R_3$	1–15–21	7–15–18	6–15–16	1–15–16	7–15–17	9–15–16	10–15–16	7–15–20	7–15–19	13–15–16	5–15–16
K_i (nM)	27	78*–331‡	700	800	1600	1900	4000	4000	4300	7400	12300

Training set	AHO12	AHO13	AHO14	AHO15	AHO16	AHO17
$\#R_1–\#R_2–\#R_3$	7–15–16	8–15–16	4–15–16	3–15–16	2–14–16	1–14–16
K_i (nM)	15300	23000	41300	113000	501000	501500

Validation set	VHO1	VHO2	VHO3
$\#R_1–\#R_2–\#R_3$	12–15–16	11–15–16	2–15–16
Ki (nM)	5500	11200	74500

(*)[20];(‡) [21]; (**) AH03 is R enantiomer of compound 13d and AH04 is the S enantiomer of compound 7 in ref [19].

QSAR Model

One Descriptor QSAR Model

"Each of the 17 training sets (TS) and 3 validation sets (VS) *Pf*A.M1-AHOx complexes (Table 1), was prepared by *in situ* modification of the refined template crystal structure (PDB entry code 4R5V[19]) of the complex *Pf*A.M1-AHO3 as described in the Methods section.Further, the relative Gibbs free energy of the *Pf*A.M1-AHOx complex formation ($\Delta\Delta G_{com}$) was computed for each of the 20 optimized enzyme–inhibitor complexes.Table 1lists computed values of $\Delta\Delta G_{com}$ and its components as defined in Equation (7), for the TS and VS of hydroxamic acid" [19].The QSAR model explained variation in the AHOs experimental inhibitory potencies ($pK_i^{exp} = - \log_{10}(K_i^{exp})$[19]) by "correlating it with computed GFE $\Delta\Delta G_{com}$ through linear regression (Equation (8), Table 2).In addition, significant correlation obtained in this QSAR relationship permitted to determine the active bound conformation of the AHOs at the *Pf*A-M1 binding site and enabled definition of the PH4 pharmacophore. In search for a better insight into the binding affinity of AHOs towards *Pf*A-M1, we have analyzed the enthalpy ofcomplexation in gas phase $\Delta\Delta H_{MM}$ by correlating it with the pK_i^{exp}. The validity of this linear correlation (for statistical data of the regression see Table 3, Equation A) allowed assessment of the significance of inhibitor-enzyme interactions ($\Delta\Delta H_{MM}$) when solvent effect and loss of entropy of the inhibitor upon binding to the enzyme were neglected.This correlation explained about 94% of the pK_i^{exp} data variation and underlined the role of the enthalpic contribution to the binding affinity of the ligand. Similarly, the more advanced descriptor, namely the GFE of the *Pf*A.M1-AHOxcomplex formation including all components: $\Delta\Delta H_{MM}$, $\Delta\Delta TS_{vib}$ and $\Delta\Delta G_{sol}$, has been assessed (for statistical data see Table 3, Equation B). Relatively high values of the regression coefficient R^2, leave-one-out cross-validated regression coefficient R^2_{xv} and Fischer F-test of the correlation suggest strong relationship between the 3D model of inhibitor binding and the observed inhibitory potencies of the AHOs"[19].Therefore, structural information derived from the 3D models of *Pf*A.M1-AHOx complexes can be expected to lead to reliable prediction of *Pf*A-M1 inhibitory potencies for new AHOs analogs based on the QSAR model B, Table 3.

Table 2. Gibbs free energy (binding affinity) and its components for the training set of *PfA*-M1 inhibitors AHO1-17 and validation set inhibitors VHO1-3[19,20,21]. AH03 is R enantiomer of compound 13d and AH04 is the S enantiomer of compound 7 in ref [19].

Trainingset [a]	M_w [b]	$\Delta\Delta H_{MM}$ [c]	$\Delta\Delta G_{SOL}$ [d]	$\Delta\Delta TS_{Vib}$ [e]	$\Delta\Delta G_{Com}$ [f]	K_i^{Exp} [g]
	[g.mol-1]	[kcal.mol-1]	[kcal.mol-1]	[kcal.mol-1]	[kcal.mol-1]	[nM]
AHO1	345	0	0	0	0	27
AHO2	380	-8.82	20.05	-11.07	22.31	78
AHO3	316	17.89	22.09	4.46	35.52	700
AHO4	332	15.42	22.16	4.02	33.55	800
AHO5	326	29.42	-4.51	-9.65	34.57	1600
AHO6	354	16.82	23.21	0.16	39.86	1900
AHO7	354	15.37	23.95	0.25	39.07	4000
AHO8	268	34.69	-4.77	-3.46	33.38	4000
AHO9	385	38.42	1.71	2.17	37.96	4300
AHO10	348	33.81	19.29	1.19	51.91	7400
AHO11	302	35.85	22.77	3.44	55.19	12300
AHO12	331	33.54	20.57	5.056	49.05	15300
AHO13	336	32.75	22.87	0.74	54.88	23000
AHO14	288	46.29	16.40	1.79	60.89	41300
AHO15	274	47.85	16.26	3.01	61.09	113000
AHO16	232	62.44	11.85	3.02	71.26	501000
AHO17	317	55.18	15.15	3.43	66.90	501500
Validation set	M_w [b]	$\Delta\Delta H_{MM}$ [c]	$\Delta\Delta G_{SOL}$ [d]	$\Delta\Delta TS_{Vib}$ [e]	$\Delta\Delta G_{Com}$ [f]	pK_i^{pre} / pK_i^{Exp} [h]
	[g.mol-1	[kcal. mol-1]	[kcal. mol-1]	[kcal. mol-1]	[kcal. mol-1]	
VHO1	351	31.20	12.12	1.41	41.92	1.02
VHO2	354	31.80	19.71	1.01	50.49	0.97
VHO3	247	49.87	11.48	2.46	58.89	1.03

[a] for the chemical structures of the training set of inhibitors see Table 1; [b] Mw is the molar mass of inhibitors;[c]$\Delta\Delta H_{MM}$ is the relative enthalpic contribution to the GFE change related to E-I complex formation derived by MM;$\Delta\Delta H_{MM} \approx [E_{MM}\{E\text{-}I_x\} - E_{MM}\{I_x\}] - [E_{MM}\{E\text{-}I_{ref}\} - E_{MM}\{I_{ref}\}]$, Iref is the reference inhibitor AHO1; [d]$\Delta\Delta G_{sol}$ is the relative solvent effect contribution to the GFE change of E-I complex formation: $\Delta\Delta G_{sol} = [G_{sol}\{E\text{-}I_x\} - G_{sol}\{I_x\}] - [G_{sol}\{E\text{-}I_{ref}\} - G_{sol}\{I_{ref}\}]$; [e]$-\Delta\Delta TS_{vib}$ is the relative entropic contribution of inhibitor to the GFE of E-I_x complexformation: $\Delta\Delta TS_{vib} = [TS_{vib}\{I_x\}E - TS_{vib}\{I_x\}] - [TS_{vib}\{I_{ref}\}E - TS_{vib}\{I_{ref}\}]$; [f]$\Delta\Delta G_{com}$ is the overall relative GFE changeof E-I_x complex formation: $\Delta\Delta G_{com} \approx \Delta\Delta H_{MM} + \Delta\Delta G_{sol} - \Delta\Delta TS_{vib}$; [g]$K_i^{exp}$ is the experimental inhibitorypotency of *Pf*A.M1obtained from ref. [19,20,21]; [h] ratio of predicted and experimental inhibitorypotencies pK_i^{pre}/pK_i^{exp}($pK_i^{pre} = -\log_{10}K_i^{pre}$) was predicted from computed $\Delta\Delta G_{com}$ using the regression equation for *Pf*A-M1 shown in Table 3, B.

Table 3. Analysis of computed binding affinities $\Delta\Delta G_{com}$, its enthalpic component $\Delta\Delta H_{MM}$, and experimental half-maximal inhibitory concentrations $pK_i^{exp} = -\log K_i^{exp}$ of AHOs towards *Pf*A-M1[19,20,21].

Statistical Data of Linear Regression	A	B
$pKi = -0.058 \times \Delta\Delta H_{MM} + 6.979$ (A) $pKi = -0.063 \times \Delta\Delta G_{compl} + 8.003$ (B)		
Number of compounds n	17	17
Squared correlation coefficient of regression R^2	0.89	0.92
LOO cross-validated squared correlation coefficient R^2_{xv}	0.88	0.91
Standard error of regression σ	0.41	0.32
Statistical significance of regression, Fisher F-test	115.58	158.64
Level of statistical significance α	>95%	>95%
Range of activities K_i^{exp} (nM) [19,20,21]	27-501500	27-501500

The statistical data confirmed validity of the correlation Equations (A) and (B) plotted on Figure 3.The ratio $pK_i^{pre}/pK_i^{exp} \approx 1$ (the pK_i^{pre} values were estimated using correlation Equation B,Table 3) calculated for the validation setVHO1-3 documents the substantial predictive power of the complexation QSAR model from Table 2. Thus, the regression Equation B (Table 3) and computed $\Delta\Delta G_{com}$ GFEs can be used for prediction of inhibitory potencies K_i^{pre} against *Pf*A-M1 for novel AHO analogs, provided they share the same binding mode as the training set hydroxamic acidAHO1-17.

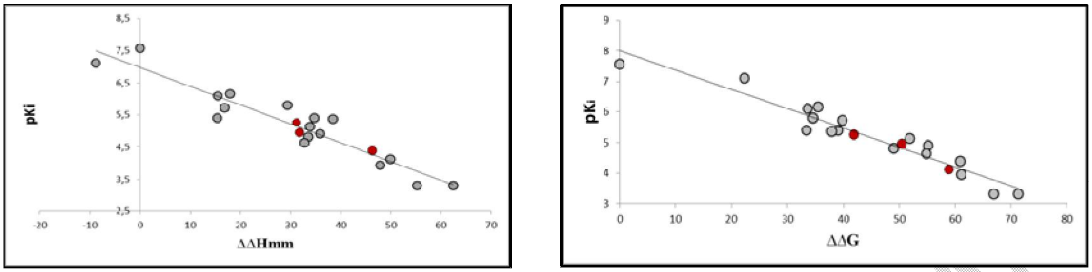

Figure 3. (Left) plot of correlation equation between pK_i^{exp} and relative enthalpic contribution to the GFE ($\Delta\Delta H_{MM}$ [kcal.mol^{-1}]). (Right) similar plot for relative complexation Gibbs free energies of the *Pf*A.M1-AHO complex formation $\Delta\Delta G_{com}$ [kcal.mol^{-1}] of the training set [19,20,21]. The validation set data points are shown in red color.

Binding Mode of AHOs

The inhibitors (AHOs) we have used throughout this work are a reported new series of hydroxamic acid obtained by synthesis [19,20,21]. Indeed, hydroxamic acids are used as metal ion chelators and the presence of the acid function in their molecular structure makes them particularly important for the inhibition of *Pf*A-M1. The reported X-rays based interaction metrics (see introduction and figure 2 for AHO3, K_i^{exp}=700 nM) are conserved as displayed on figure 4 (AHO1, K_i^{exp}=27 nM).The supplementary two hydrogen bonds between AHO1 and the residues Glu497 and Ala461 along with a π-stacking interaction with Tyr580 and finally a deeper hydrophobic contact with S1 substantially result in the 26-fold increase of potency from AHO3 to AHO1.

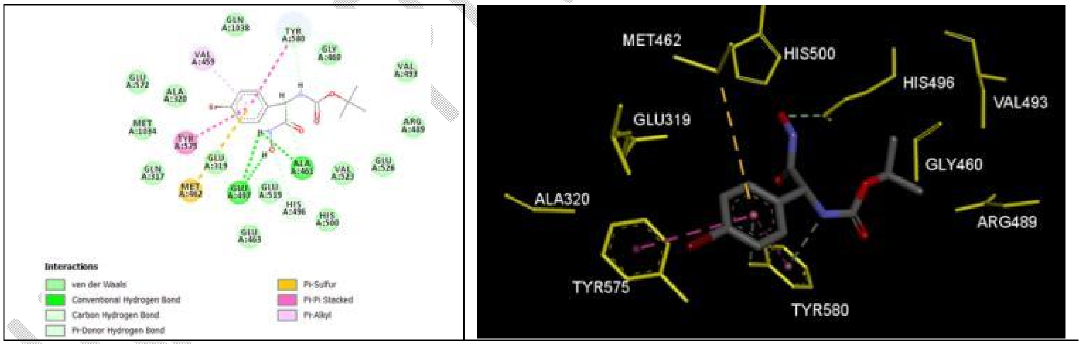

Figure 4. (Left) 2D schematic interaction diagram of the most potent inhibitor AHO1 at the active site of *Pf*A-M1 and (Right) 3D schematic interaction of AHO1 at the enzyme active site

Interaction Energy

The energetic understanding of the different ligands (AHOx) used in the inhibition of *Pf*A-M1 is also provided by the energy interaction diagram (IE; ΔE_{int}). The distribution of the interaction energy in contribution of the residues to the active site of *Pf*A-M1 is done in three classes: a first class of ligands with maximum biological activity (figure 5), a second class of ligands with moderate biological activity and a third class of ligands with lowest biological activities.

Forall classes, the interaction energy per residue is stronger with the residues Tyr580, Tyr575 and Glu497, and they are moderated with the catalytic triad His500, His496 and Glu519 as reported by Shailesh *et al.*[**Error! Bookmark**

not defined.].It's interesting to analyze inside class 1, the difference of residue contribution to interaction energy from the diagram in Figure 5, (top, A): AHO1 (K_i^{exp}=27 nM) values in blue are compared with those of AHO3 (K_i^{exp}=700 nM) in green while Tyr580 and Tyr575 contribution is -2 kcal.mol^{-1} and -1 kcal.mol^{-1} respectively in favor of AHO3, the trend is inversed for Met462, Glu497, His500, Glu519 and Glu526 with -1, -1, -1.5, -1.5, -1.5 kcal.mol^{-1} respectively resulting in almost -3.5 kcal.mol^{-1} in favor of AHO1.In contrast, no relevant greatdifference is noticeable from class 1 to class 3 via class 2. Therefore in the lack of structural substitution directed to any active site residue, only a virtual screening of a diverse combinatorial library is expected to bring to novel more potent AHO analogsexpecting that stabilizing supplementary interaction from favorable sidechains' rotation involving residues not displayed in this representation will occur.

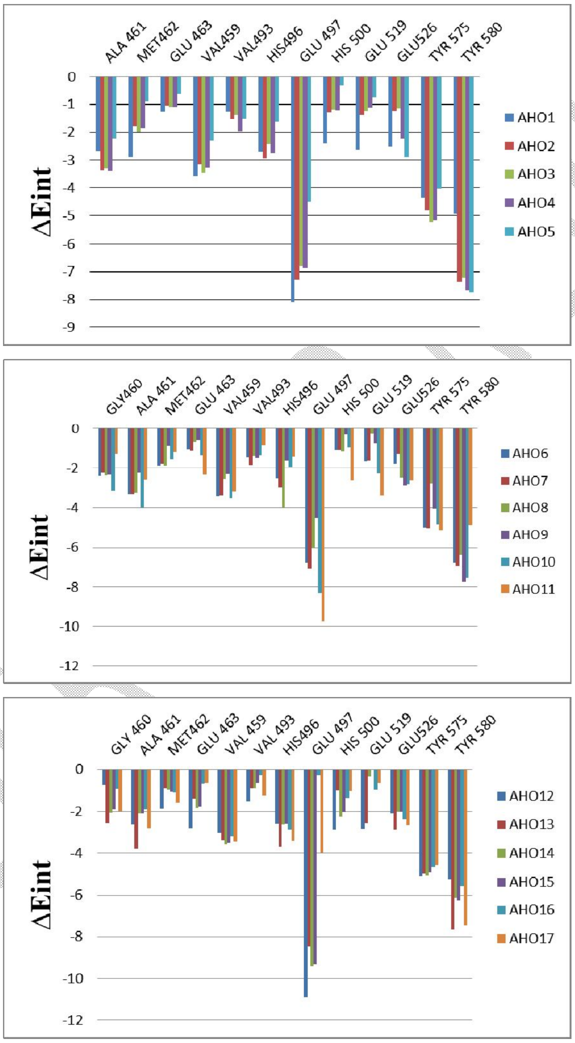

Figure 5. Molecular Mechanics intermolecular interaction energy E_{int} breakdown to residue contributions in [kcal.mol^{-1}]: (A:**Top**) the most active inhibitors AHO1-4, (B:**Middle**) moderately active inhibitors AHO5-8, (C:**Bottom**) less active inhibitors AHO9-12, Table 2 [**Error! Bookmark not defined.**].

3D-QSAR Pharmacophore Model

Generation and Validation of 3D-QSAR Pharmacophore

*Pf*A-M1 inhibition 3D-QSAR pharmacophore was generated from the active conformation of 17TS AHO1-17 and evaluated by 3 VS VHO1-3 covering a large range of experimental activity(27–501500 nM) spanning almost fourorders of magnitude. The generation process is divided into three main steps: (i) the constructive step, (ii) the subtractive step, and (iii) the optimization step [26] as described earlier. Accordingly, none of the training set AHOx was inactive and no starting PH4 features were removed. Finally, during the optimization phase, the score of the pharmacophoric hypotheses was improved. Hypotheses were scored according to errors in activity estimates from regression and complexity via a simulated annealing approach. At the end of the optimization, the top scoring 10 unique pharmacophore hypotheses were kept, all displaying five-pointfeatures. The cost values, correlation coefficients, root-mean square deviation (RMSD) values, the pharmacophore features, and the max-fit value of the top 10 ranked hypotheses (Hypo1-Hypo10) are listed in Table 4. They were selected based on significant statistical parameters, such as high correlation coefficient, low total cost, and low RMSD.

Table 4. Parameters of 10 generated PH4 pharmacophoric hypotheses for PfA-M1 inhibitor after Cat-Scramble validation procedure (49 scrambled runs for each hypothesis at the selected level of confidence of 98%).

Hypothesis	RMSD [a]	R^2 [b]	Total Costs [c]	Costs Difference [d]	Closest Random [e]
Hypo1	3.405	0.950	156.5	814.0	149.88
Hypo2	3.414	0.949	156.9	813.6	223.83
Hypo3	3.884	0.893	231.3	739.2	230.94
Hypo4	5.099	0.883	248.3	722.2	234.95
Hypo5	5.098	0.882	248.4	722.1	240.84
Hypo6	5.208	0.877	257.1	713.4	245.43
Hypo7	5.391	0.867	272.7	697.8	245.78
Hypo8	5.695	0.851	299.6	670.9	246.23
Hypo9	5.745	0.849	304.2	666.3	248.86
Hypo10	5.747	0.848	304.4	597.5	262.49

[a] root means square deviation; [b] squared correlation coefficient; [c] overall cost parameter of the PH4 pharmacophore; [d] cost difference between Null cost and hypothesis total cost; [e] lowest cost from 49 scrambled runs at a selected level of confidence of 98%. The Fixed Cost = 40.1 with RMSD = 0, the Null Cost = 970.5 with RMSD = 10.852 and the Configuration cost = 10.67

The generated pharmacophore models were then assessed for their reliability based on the calculated cost parameters ranging from 45.8 (Hypo1) to 59.6 (Hypo10). The relatively small gap between the highest and lowest cost parameter corresponds well with the homogeneity of the generated hypotheses and consistency of the TS of AHOx. For this PH4 model, the fixed cost (40.1) is lower than the null cost (970.5) by a difference $\Delta = 930.7$. This difference is a major quality indicator of the PH4 predictability ($\Delta > 70$ corresponds to an excellent chance or a probability higher than 90% that the model represents a true correlation [26]). To be statistically significant, a hypothesis has to be as close as possible to the fixed cost and as far as possible from the null cost. For the set of 10 hypotheses, the difference $\Delta \geq 373.0$, which attests to the high quality of the pharmacophore model. The standard indicators such as the RMSD between the hypotheses ranged from 3.405 to 5.747, and the squared correlation coefficient (R^2) falls to an interval from 0.95 to 0.84. The first PH4 hypothesis with the closest cost (156.5) tothe fixed one (40.1) and best RMSD and R^2 was for further analysis. Statistical data for the set of hypotheses (costs, RMSD, R^2) are listed in Table 4. The configuration cost (10.67 for all hypotheses) far below 17 confirms this pharmacophore as a reasonable one.

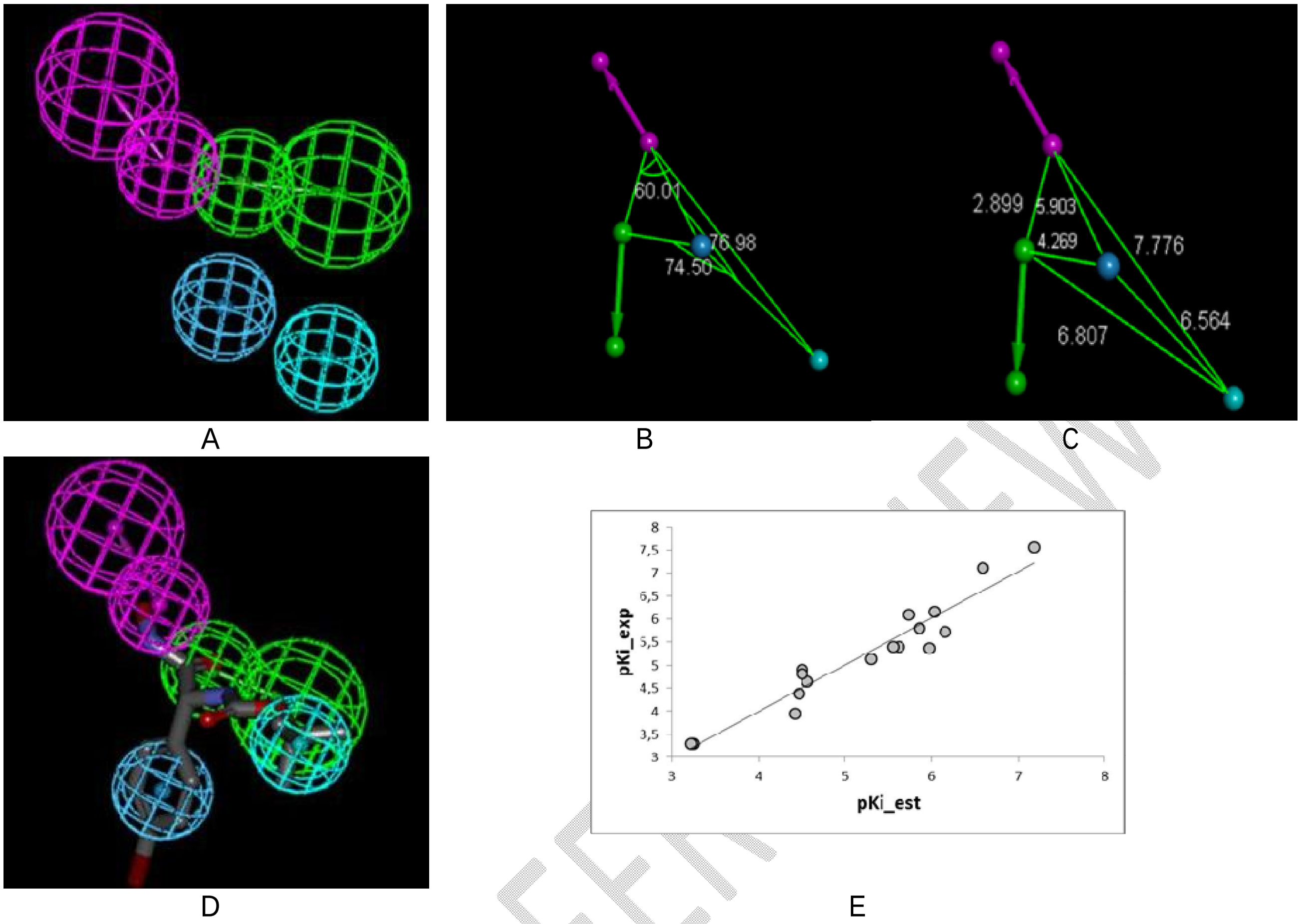

Figure 6. Features (**A**) coordinates of centers, (**B**) angles between centers of pharmacophoric features, (**C**) distances between centers, (**D**) mapping of pharmacophore of *Pf*A-M1 inhibitor with the most potent molecule AHO1. Feature legend: HYDA = Hydrophobic Aliphatic (blue), HYD = Hydrophobic (cyan), HBA = Hydrogen bond Acceptor (green). (**E**) Correlation plot of experimental vs. predicted inhibitory activity (open circles correspond to TS, red dots to VS).

We can carry out computational design and selection ofnewAHOanalogs with elevated inhibitorypotencies against *Pf*A-M1, based on a strategy using the noticeable presence of the hydrophobic featuresincluded in the best pharmacophore model at the position of R2 coupled with mapping of R3 to thearomatic ring feature and the appropriate ring substitution to the hydrophobic aliphatic feature inHypo1 (Figure 5).

Virtual Screening

In silico screening of a virtual (combinatorial) library can lead to hit identification as it was shown in our previous works on inhibitors design [39].

Virtual Library

An initial virtual library (VL) was generated by substitutions at positions for R1,R2 and R3 (see Table 5) on the Phenylscaffold. During the virtual library enumeration, all 149 R-groups (3-151) and two (2) R1 listed in Table 5 were attached to in positions R1, R2 and R3 of the AHO scaffold to enumerate a combinatorial library of the size: R1 × R2 × R3 = 2×149×149 = 44,402focused to 12,210analogs fulfilling the Lipinski's rule of five [40]. This initial diversity library was generated from building blocks (chemicals) listed in the databases of available chemicals.

Table 5. R_1, R_2 and R_3-groups (fragments, building blocks, substitutents) used in the design of the initial diversity virtual combinatorial library.

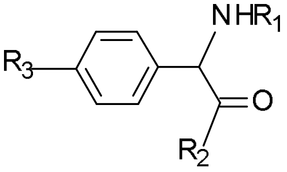

R_1: 1---NHOH ; 2---OH							
R_2or R_3							
3	1-formylcyclopenta-2,4-dien-1-yl	**4**	1-formyl-2-methylcyclo-penta-2,4-dien-1-yl	**5**	2-fluoro-1-formylcyclopenta-2,4-dien-1-yl	**6**	2-amino-1-formylcyclopenta-2,4-dien-1-yl
7	1-formyl-2-mercaptocyclopenta-2,4dien-1-yl	**8**	1-formyl-3-mercaptocyclopenta-2,4-dien-1-yl	**9**	1-formyl-2,3-dimercaptocyclopenta-2,4-dien-1-yl	**10**	2-chloro-1-formylcyclopenta-2,4-dien-1-yl
11	3-chloro-1-formylcyclopenta-2,4-dien-1-yl	**12**	2,3-dichloro-1-formylcyclopenta-2,4-dien-1-yl	**13**	3-bromo-1-formylcyclopenta-2,4-dien-1-yl	**14**	2-bromo-1-formylcyclopenta-2,4-dien-1-yl
15	2,3-dibromo-1-formylcyclopenta-2,4-dien-1-yl	**16**	1-formyl-2-iodocyclopenta-2,4-dien-1-yl	**17**	1-formyl-3-iodocyclopenta-2,4-dien-1-yl	**18**	1-formyl-2,3-diiodocyclopenta-2,4-dien-1-yl
19	1-aminomethyl-cyclopenta-2,4-dien-1-yl	**20**	1-aminomethyl-2-fluorocyclopenta-2,4-dien-1-yl	**21**	1-aminomethyl-2,3-difluorocyclopenta-2,4-dien-1-yl	**22**	1-aminomethyl-2-mercaptocyclopenta-2,4-dien-1-yl
23	1-aminomethyl-2,3-dimercaptocyclopenta-2,4-dien-1-yl	**24**	2,3-dimercapto-1-mercaptoamino-methyl-cyclopenta-2,4-dien-1-yl	**25**	2-mercapto-1-mercaptoamino-methyl-cyclopenta-2,4-dien-1-yl	**26**	3-mercapto-1-mercaptoamino-methyl-cyclopenta-2,4-dien-1-yl
27	3-fluoro-1-mercaptoamino-methyl-cyclopenta-2,4-dien-1-yl	**28**	2-fluoro-1-mercaptoaminomethyl-cyclopenta-2,4-dien-1-yl	**29**	2,3-difluoro-1-mercaptoamino-methyl-cyclopenta-2,4-dien-1-yl	**30**	1-fluoroamino-methyl-2,3-dimercaptocyclopenta-2,4-dien-1-yl
31	1-fluoroamino-methyl-2-mercaptocyclopenta-2,4-dien-1-yl	**32**	1-fluoroamino-methyl-3-mercaptocyclopenta-2,4-dien-1-yl	**33**	3-fluoro-1-fluoroamino-methyl-cyclopenta-2,4-dien-1-yl	**34**	2,3-difluoro-1-fluoroamino-methyl-cyclopenta-2,4-dien-1-yl
35	2,3-dichloro-1-fluoroamino-methyl-cyclopenta-2,4-dien-1-yl	**36**	2-chloro-1-fluoroamino-methyl-cyclopenta-2,4-dien-1-yl	**37**	3-chloro-1-fluoroamino-methyl-cyclopenta-2,4-dien-1-yl	**38**	3-bromo-1-fluoroamino-methyl-cyclopenta-2,4-dien-1-yl
39	2,3-dibromo-1-fluoroamino-methyl-cyclopenta-2,4-dien-1-yl	**40**	2-bromo-1-fluoroamino-methyl-cyclopenta-2,4-dien-1-yl	**41**	2-oxo-1-phenylethyl	**42**	3-aminomethyl-2-oxo-1-phenylethyl
43	5-aminomethyl-2-oxo-1-phenylethy	**44**	5-aminomethyl-2-chloro-2-oxo-1-phenylethyl	**45**	2-amino-5-aminomethyl-2-oxo-1-phenylethyl	**46**	2-carbamoyl-2-oxo-1-phenylethyl
47	5-carbamoyl-2-oxo-1-phenylethyl	**48**	4-carbamoyl-2-oxo-1-phenylethyl	**49**	6-mercaptobenzoic-acid-2-oxo-1-phenylethy	**50**	5-mercaptobenzoic-acid-2-oxo-1-phenylethy
51	4-mercaptobenzoic-acid-2-oxo-1-phenylethy	**52**	2,3-dimercaptobenzoic-acid-2-oxo-1-phenylethy	**53**	2-iminomethyl-oxo-1-phenylethy	**54**	2-iminomethyl-phenyl
55	3-iminomethyl-phenyl	**56**	4-iminomethyl-phenyl	**57**	2-iminomethyl-3-mercaptophenyl	**58**	2-iminomethyl-3,4-dimercaptophenyl
59	2-iminomethyl-2-mercapto-phenyl	**60**	2-iminomethyl-4-mercapto-phenyl	**61**	3-fluoro-2-iminomethyl-phenyl	**62**	4-fluoro-2-iminomethyl-phenyl
63	4-bromo-2-iminomethyl-phenyl	**64**	3-bromo-2-iminomethyl-phenyl	**65**	2-chloro-2-iminomethyl-phenyl	**66**	3-chloro-2-iminomethyl-phenyl
67	4-chloro-2-iminomethyl-phenyl	**68**	4-bromo-2-bromoimino-methyl-phenyl	**69**	4-chloro-2-chloroimino-methyl-phenyl	**70**	3-chloro-2-chloroimino-methyl-phenyl
71	2-chloroimino-methyl-3-methylphenyl	**72**	2-chloroimino-methyl-3-trifluoromethyl-phenyl	**73**	2-chloroimino-methyl-4-trifluoromethyl-phenyl	**74**	2-formyl-4-methylphenyl
75	2-formyl-2-oxo-1-phenylethyl	**76**	3-formyl-2-oxo-1-phenylethyl	**77**	2-formyl-3-mercaptophenyl	**78**	2-formyl-3,4-dimercaptophenyl
79	2-formyl-4-mercaptophenyl	**80**	2-formyl-2-mercaptophenyl	**81**	6-methylbenzoyl-2-oxo-1-phenylethyl	**82**	6-trifluoromethylbenzoyl-2-oxo-1-phenylethyl
83	5-trifluoromethylbenzoyl-2-oxo-1-phenylethyl	**84**	2-fluoro-2-oxo-1-phenylethyl	**85**	2-aminofluoromethyl-6-bromo-2-oxo-1-phenylethyl	**86**	2-ureidoacetamide
87	4-chloro-1H-pyrazol-1-yl	**88**	4,5-dichloro-1H-pyrazol-1-yl	**89**	5-chloro-1H-pyrazol-1-yl	**90**	3-chloro-1H-pyrazol-1-yl
91	3-bromo-1H-pyrazol-1-yl	**92**	4-bromo-1H-pyrazol-1-yl	**93**	3,4-bromo-1H-pyrazol-1-yl	**94**	5-bromo-1H-pyrazol-1-yl
95	4,5-dibromo-1H-pyrazol-1-yl	**96**	3,4,5-tribromo-1H-pyrazol-1-yl	**97**	4,5-dimercapto-1H-pyrazol-1-yl	**98**	5-mercapto-1H-pyrazol-1-yl
99	5-iodo-1H-pyrazol-1-yl	**100**	4-iodo-1H-pyrazol-1-yl	**101**	3-iodo-1H-pyrazol-1-yl	**102**	3,4-diiodo-1H-pyrazol-1-yl
103	3,4,5-triiodo-1H-pyrazol-1-yl	**104**	3,4,5-trifluoro-1H-pyrazol-1-yl	**105**	3-trifluoro-1H-pyrazol-1-yl	**106**	3,4-difluoro-1H-pyrazol-1-yl
107	4-fluoro-1H-pyrazol-1-yl	**108**	5-fluoro-1H-pyrazol-1-yl	**109**	3-amino-1H-pyrazol-1-yl	**110**	4-amino-1H-pyrazol-1-yl
111	5-amino-1H-pyrazol-1-yl	**112**	5-methyl-1H-pyrazol-1-yl	**113**	5-ethyl-1H-pyrazol-1-yl	**114**	4-methyl-1H-pyrazol-1-yl
115	4,5-dimethyl-1H-pyrazol-1-yl	**116**	5-mercaptomethyl-1H-pyrazol-1-yl	**117**	4-mercapto-5-mercapto-methyl-1H-pyrazol-1-yl	**118**	5-aminothio-4-mercapto-1H-pyrazol-1-yl)
119	4,5-bis-aminothio-1H-pyrazol-1-yl	**120**	4,5-bis-aminothio-3-mercapto-1H-pyrazol-1-yl	**121**	5-ethyl-4-methyl-1H-pyrazol-1-yl	**122**	2-phenylamino
123	2-pyridin-4-ylamino	**124**	2-pyridin-3-ylamino	**125**	2-pyridin-2-ylamino	**126**	2-pyridazin-3-ylamino
127	3-pyridazin-3-ylamino	**128**	2-pyridazin-4-ylamino	**129**	2-phenyl-2-pyridazin-3-ylamino	**130**	3-phenyl-2-pyridazin-3-ylamino

131	3-methylpyrazin-2-yl	**132**	4-methylpyrazin-2-yl	**133**	2-methylpyrazin-2-yl	**134**	3-ethylpyrazin-2-yl
135	4-ethylpyrazin-2-yl	**136**	2,3-dimethylpyrazin-2-yl	**137**	5-ethylpyrimidine-2,4,6(1H,3H,5H)-trionyl	**138**	1,3,5,7tetraazatricyclo[3.3.1.13,7]decanyl hexaméthylène- tétramine
139	2,3-difluoro-5-methyl-N-(trifluoromethyl)cyclopenta-1,3-dien-1-aminyl	**140**	[(2,3-difluorocyclopenta-1,3-dien-1-yl)amino] methanetriol	**141**	benzenesulfonamidyl	**142**	N-tert-butyl-2,3-difluorocyclopenta-1,3-dien-1-aminyl
143	1-aminoéthane-2,2-diolyl	**144**	3,3-dihydroxypropanoyl fluoride	**145**	1,1,1-trifluoropropane-2,2-diolyl	**146**	ethane-1,1,1-triolyl
147	2,3-difluorocyclopenta-1,3-dienyl	**148**	C(O)^{t}Bu	**149**	Boc	**150**	methylcubane
151	O^{t}Bu						

In Silico Screening of Library of AHOs

The focused library of 44,402analogs was further screened for molecular structures matchingthe 3D-QSAR PH4 pharmacophore model Hypo1 of *Pf*A-M1 inhibition. 51AHOs mapped to at least 4 features of the pharmacophore. Thesebest fitting analogs (PH4 hits) then underwent complexation QSAR model screening. The computedGFE of *Pf*AM1-AHOx complexformation, their components, and predicted half-maximal inhibitory concentrations K_i^{pre} calculated from the correlation equation B (Table 3) are listed in table 6.

Table 6. GFE and their components for the top scoring 51 virtual AHO analogs. The analog numbering concatenates the index of each substituent R1 to R3 with the substituent numbers taken from Table 5 except for hydrogen which is directly specified by the letter H

	Analogs	M_w^{a} [g.mol^{-1}]	$\Delta\Delta H_{MM}$ ^{b} [kcal. mol^{-1}]	$\Delta\Delta G_{SOL}$^{c} [kcal. mol^{-1}]	$\Delta\Delta TS_{Vib}$^{d} [kcal. mol^{-1}]	$\Delta\Delta G_{Com}$ ^{e} [kcal. mol^{-1}]	K_i^{pred} ^{f} [nM]
	AHO1	345	0	0	0	0	27
1	1-140-141	498	-4.97	-10.04	-4.13	-10.88	2.1
2	1-142-141	492	4.97	-14.09	1.03	-10.14	2.3
3	1-150-141	465	5.15	-13.16	-1.22	-6.78	3.8
5	1-148-141	405	10.86	-16.68	-0.74	-5.08	4.8
6	1-149-141	421	10.83	-15.06	0.83	-5.05	4.8
7	1-151-141	393	11.70	-16.11	-1.29	-3.12	6.3
8	1-6-50	425	14.54	-11.78	-4.40	7.15	28
9	1-7-77	427	16.93	-11.19	-2.88	8.63	34.7
10	1-5-135	376	75.31	-60.40	0.19	14.72	83.8
11	1-10-65	403	33.05	-18.84	-2.50	16.71	111.7
12	1-3-41	394	41.81	-23.13	1.86	16.82	113.6
13	1-8-44	461	70.54	-55.65	-2.74	17.63	127.7
14	1-12-108	375	32.94	-16.30	-1.64	18.28	140.3
15	1-8-134	376	-46.22	66.92	2.07	18.64	147.7
16	1-11-81	394	38.99	-19.67	0.46	18.85	152.3
17	1-11-28	418	37.06	-19.63	-1.86	19.29	162.4
18	1-3-89	360	37.48	-19.74	-1.71	19.45	166.2
19	1-8-61	402	35.68	-19.51	-3.86	20.03	180.6
20	1-9-121	431	19.39	2.37	0.54	21.21	214.4
21	1-4-82	390	35.68	-13.98	-0.06	21.75	231.9
22	1-4-67	472	40.32	-19.51	-1.79	22.61	262.4
23	1-4-136	360	3.13	23.52	3.34	23.32	290.9
24	1-6-70	385	14.00	9.68	-0.43	24.10	326
25	1-12-129	379	43.74	-19.03	-0.11	24.83	362
26	1-3-122	337	19.09	8.44	1.55	25.98	427.7
27	1-3-63	413	45.59	-19.25	-0.48	26.81	482.6
28	1-12-106	396	38.40	-11.08	0.12	27.20	510.5
29	1-5-128	358	17.83	9.74	-0.13	27.70	548.4
30	1-11-62	405	44.73	-19.53	-2.61	27.81	557.8
31	1-4-70	410	45.97	-19.04	-1.98	28.91	653.6
32	1-3-86	360	47.48	-20.41	-1.71	28.78	641.7
33	1-7-95	593	13.97	7.57	-7.88	29.42	704.3
34	1-12-13	437	-11.36	36.43	-4.90	29.97	762.4
35	1-3-106	361	14.54	14.88	-1.95	31.37	933
36	1-6-120	436	30.38	1.69	-0.31	32.39	1082

	Analogs	M_w[a] [g.mol^{-1}]	$\Delta\Delta H_{MM}$[b] [kcal. mol^{-1}]	$\Delta\Delta G_{SOL}$[c] [kcal. mol^{-1}]	$\Delta\Delta TS_{Vib}$[d] [kcal. mol^{-1}]	$\Delta\Delta G_{Com}$[e] [kcal. mol^{-1}]	K_i^{pred}[f] [nM]
37	1-10-20	404	51.09	-17.33	0.55	33.21	1218.4
38	1-4-117	417	21.67	13.97	-1.22	36.87	2069.5
39	1-10-93	437	14.22	19.49	-4.74	38.45	2603.3
40	1-8-113	384	17.41	25.39	3.30	39.49	3026.6
41	1-4-59	408	58.97	-18.30	0.34	40,33	3416.4
42	1-4-32	398	55.92	-12.68	1.83	41.41	3994.5
43	1-12-120	487	-1.03	45.92	2.46	42.42	4628.7
44	1-8-87	391	21.59	20.86	-1.28	43.73	5596.6
45	1-9-102	640	14.66	22.56	-7.16	44.38	6147.4
46	1-6-65	384	64.20	-17.03	0.53	46.65	8533.7
47	1-11-82	419	60.12	-14.46	-3.68	49.34	12611.4
48	1-4-63	427	68.07	-20.03	-2.09	50.13	14137.2
49	1-3-79	394	70.80	-19.35	-1.02	52.46	19817.2
50	1-3-37	369	75.97	-21.52	1.53	52.92	21165.8
51	1-4-131	352	77.48	-22.48	-0.38	5.37	30201.7

[a] M_w is molar mass of inhibitor; [b]$\Delta\Delta H_{MM}$ is the relative enthalpic contribution to the GFE change of the *Pf*A-M1-AHO complex formation $\Delta\Delta G_{com}$ (for details see footnote pf Table 2); [c]$\Delta\Delta G_{sol}$ is the relative solvation GFE contribution to $\Delta\Delta G_{com}$; [d]$\Delta\Delta TS_{vib}$ is the relative (vibrational) entropic contribution to $\Delta\Delta G_{com}$; [e]$\Delta\Delta G_{com}$ is the relative Gibbs free energy change related to the enzyme–inhibitor *Pf*A-M1-AHO complex formation $\Delta\Delta G_{com} \equiv \Delta\Delta H_{MM} + \Delta\Delta G_{sol} - \Delta\Delta TS_{vib}$; [f] K_i^{pre} is the predicted inhibition potency towards PfA-M1 calculated from $\Delta\Delta G_{com}$ using correlation Equation B, Table 3; g K_i^{exp} [**Error! Bookmark not defined.**]is given for the reference inhibitor AHO1 instead of the K_i^{pre}.

Novel AHO Analogs

The PH4-based screening of theAHO analogs virtual library resulted in novel identified compounds with better predicted potency. The analysis of frequency of occurrence of R-group during the selection of appropriate surrogates for two points of attachment: R2-group and R3-group since in R1 the amino group is the unique to be represented. The frequency of occurrence of groups R2 and R3 among the best resulting from PH4 (figure 7) is as follow: forS1' filling R2-groups, 3: 1-formylcyclopenta-2,4-dien-1-yl, 4: 1-formyl-2-methylcyclopenta-2,4-dien-1-yl, 9: 1-formyl-2,3-dimercaptocyclopenta-2,4-dien-1-yl, and 11: 3-chloro-1-formylcyclopenta-2,4-dien-1-yl,with occurrences of 9, 8, 5, 5 respectively are the most represented while 140: [(2,3-difluorocyclopenta-1,3-dien-1-yl)amino] methanetriol, 149: Boc, 150: methylcubane, 148: C(O)^{t}Bu, and 151: O^{t}Bu), all with occurrence of one, appear in the highest potency AHO analogs. In the S1 filling R3-group position 141: Benzenesulfonamidyl with occurrence of 6 is the most represented, appearing in all the top 6 highest potency AHO analogs. The best analogs from these most commonly used substitutents (R2-group: R3-group) are: 1-140-141 (K_i^{pre} = 2.1nM); 1-142-141 (K_i^{pre} = 2.3 nM); 1-149-141 (K_i^{pre} = 4.8nM); 1-150-141 (K_i^{pre} = 3.8nM); 1-148-141 (K_i^{pre} =4.8 nM); 1-151-141 (K_i^{pre} = 6.3 nM). Branching larger aliphatic moieties in the R_2 and R_3 positions of the AHO analogs contributed strongly to an overall improvement in the inhibitory activity of *PfA*-M1. This relates to the inhibitory potency of the best proposed new analogs. For example, the proposed analog 1-140-141 has an inhibitory concentration of 2.1 nM, approximately 13 times less than the most active compound in the proposed TS series (27 nM) by Shailesh et al. [19].

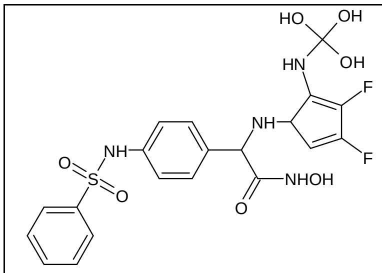

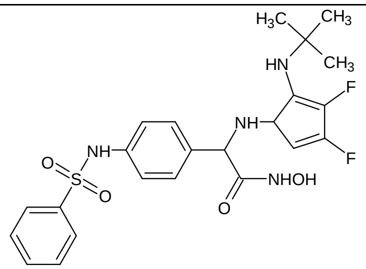

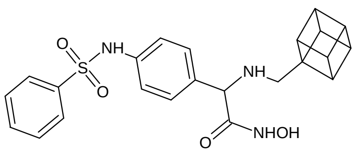

1-140-141 : Ki=2.1 nM	1-142-141 : Ki=2.3 nM	1-150-141 : Ki=3.8 nM
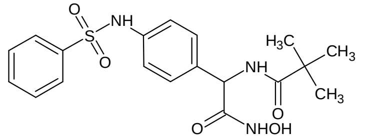	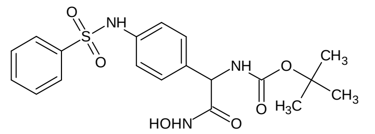	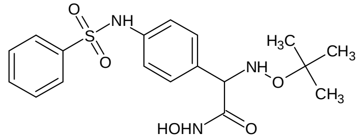
1-148-141 : Ki= 4.8 nM	1-149-141 : Ki= 4.8 nM	1-151-141 : K= 6.3 nM

Figure 7. The best AHO Analogs with scaffold of *Pf*A-M1, the name is a concatenation #R1-#R2-#R3

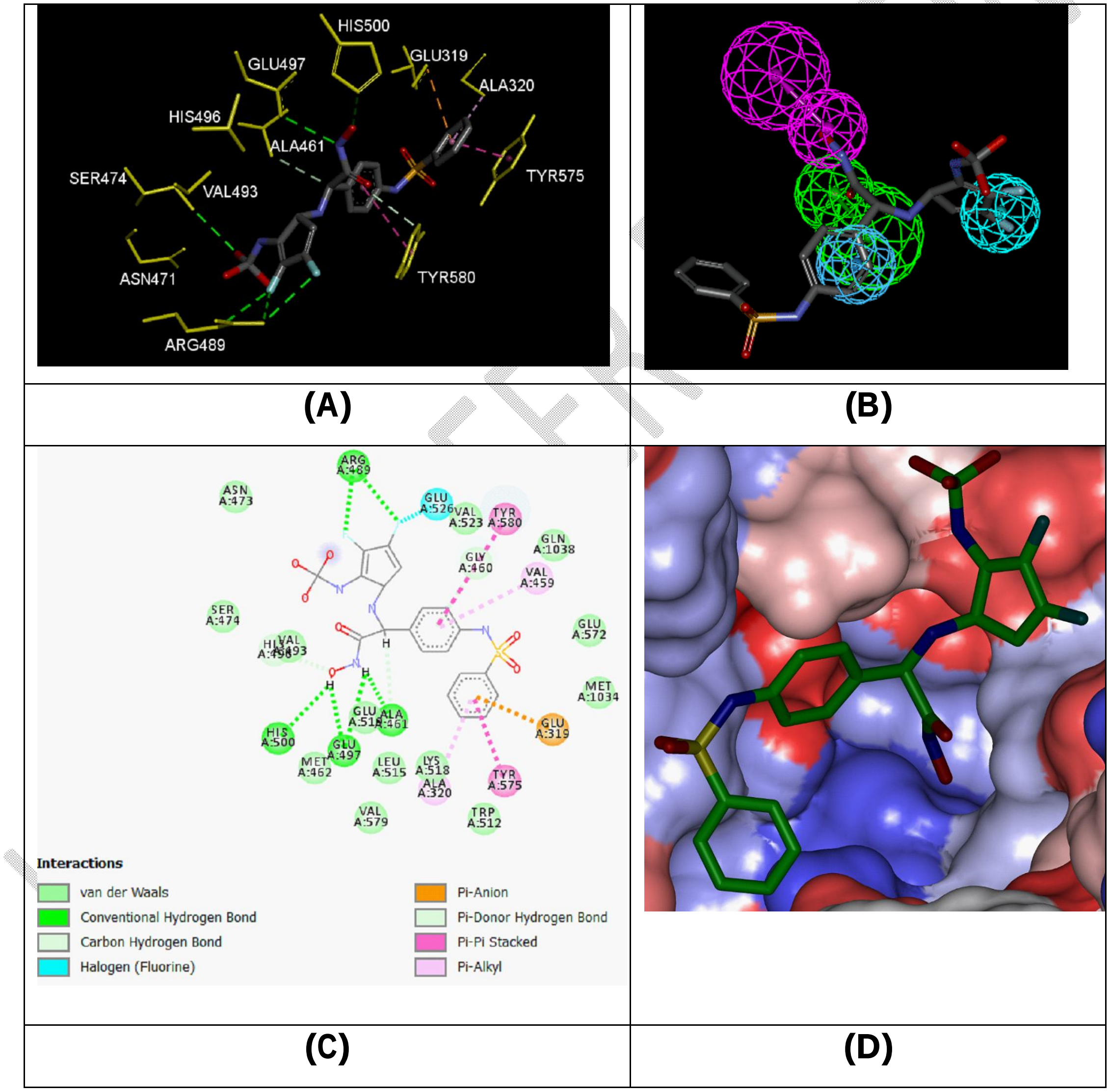

Figure 8. (**A**) Close up of virtual hit 1-140-141, the most active designed AHO analog (K_i^{pre} = 2.1 nM) at the active site of *Pf*A-M1. (**B**) Mapping of the AHO 1-140-141 to *Pf*A-M1 inhibition pharmacophore. (**C**) 2D schematic interaction diagram of the best active designed AHO analog 1-140-141 at the active site of *Pf*A-M1. (**D**) Surface of the active site of *Pf*A-M1 with bound best active designed AHO analog. The binding site surface is colored according to residue hydrophobicity: red = hydrophobic, blue = hydrophilic, and white = intermediate.

Pharmacokinetic Profile of Novel AHO Analogs

For decades, the question of the pharmacokinetic profile has been a very important issue in the search for new inhibitors, particularly *Pf*A-M1 inhibitors [41]. One of the compounds studied was triclosan with very low oral bioavailability due to its low water solubility and rapid phase II metabolism, which must be optimized for possible use as an antituberculosis drug, possibly as an antimalarial drug in cases of high affinity with *Pf*EACP [42]. Table 7 as presented below shows the properties related to ADME, including octanol-water partition coefficient, aqueous solubility, blood-brain partition coefficient, Caco-2 cell permeability, serum protein binding, number of probable metabolic reactions and eighteen other descriptors related to the absorption, distribution, metabolism and excretion (ADME) of new analogs. In addition, these properties were calculated by the QikProp programme [37]on the basis of Jorgensen's method [43, 44]. In the search for new inhibitors, more than 500 drugs from around 710 compounds have been used to obtain regression equations correlating experimental and calculated descriptors, which gives an accurate prediction of the pharmacokinetic properties of the molecules. The oral bioavailability predicted for the new AHOanalogs is 85% higher thanthat of triclosan, where the best activederivativehas an unfavorable oral bioavailability. Since a value above 80% is considered good, about ten AHOanalogs show a human oral absorption in the gastrointestinal tract (HOA) of 100%. Drug-like (#stars) - the number of property descriptors that fall outside the range of optimal values determined for 95% of known drugs out of 24 selected descriptors calculated by QikProp was used as an additional selection criterion for ADME-related compounds. The values for the best designed AHOs are compared with those calculated for drugs used for the treatment of malaria or in clinical trials (Table7). Our best-designed analogs all show #stars equal to zero, meaning that the optimal range of values for none of the descriptors of drug dependence was violated. Thus, designed AHOs have a much more interestingpharmacokinetic profile in the development of *Pf*A-M1 inhibitors.

Table 7. ADME-related properties of the best designed analogs and known antipaludic agents either in clinical use or currently undergoing clinical testing computed by QikProp [37].

AHO [a]	# stars[b]	M_W[C] [g.mol^{-1}]	S.mol [d] [Å^2]	Smolhfo[e] [Å^2]	V mol[f] [Å^3]	RotB[g]	HB_{don}[h]	HB_{acc}[i]	Log [j] p_o/w
1-142-141	0	493	789.9	209.4	1445.1	10	5	11.2	0.7
1-140-141	2	498	757.9	27.5	1356.9	13	8	11.2	-1.2
1-149-141	0	422	705.2	203.9	1283.3	8	3.3	10.5	0.7
1-151-141	0	393	641.1	174.5	1187	9	4	10.1	0.3
1-148-141	0	405	696.7	205.6	1253.1	8	3.3	10.5	0.1
1-150-141	0	466	638.8	193.9	1265.5	9	3.3	10.5	0.1
Dapsone	1	236	431.6	0	687.9	2	0	7	-0.4
Trimethoprim	0	272	500.2	223.9	835.9	5	0	6.5	0.6
Chloroquine	1	294	594.2	188.9	982.9	6	0	3	4.6
Amodiaquine	1	334	603.2	131.7	1018.7	6	0	5	3.6
Mefloquine	2	362	533.1	0	925.1	2	0	4	4.1
Pamaquin	0	316	655	443.4	1148.1	9	1	4.75	4.1
Sulfametopyrazin	1	268	473.4	77.8	773.3	4	0	9	-1.1
Tetracyclin	5	422	604.5	173.1	1111.8	2	0	16	-3.4
Quinacrin	0	370	680.5	268.8	1163.6	7	0	3.5	5.6
Proguanil	1	238	478.2	125.3	768.6	6	0	6	1.1
Halofantrine	5	470	785.4	160.2	1351.8	5	0	3	7.6
Sulfadoxine	1	296	510.6	152.3	849.5	5	0	9.5	-0.8
Hydroxychloroquin	1	310	609.5	119.5	1006.5	6	0	5	3.4
Buloquin	0	400	560.2	360.2	1097.8	9	1	5.8	3.6
Lumefantrin	5	497	819.1	160.7	1437.5	7	0	3	8.3
Arteether	1	312	531.1	506.1	970.2	2	0	5.7	2.7

Dihydroartemisinine	1	384	477.4	395.7	864.6	1	1	5.7	1.8
Doxycyclin	4	422	602.2	174.1	1104.2	2	0	17.2	-3.9
Artemisinin	0	282	456.6	380.6	848.4	0	0	5.3	1.7

(Table 7 continued)

AHO [a]	Log swat[k]	Log KHSA[l]	Log B/B[m]	BIPcaco[n] [nm.S^{-1}]	#meta [o]	K_i^{pred}	HOA [q]	% HOA[r]
1-142-141	-1.9	-0.48	-1.3	4.2	4	2.3	2	42.2
1-140-141	-0.6	-0.9	-2.9	0.2	3	2.1	1	0
1-149-141	-3	-0.6	-2.4	23	1	4.8	2	55.7
1-151-141	-1.9	-0.8	-2.1	39.2	1	6.3	2	57.2
1-148-141	-2.4	-0.9	-2.3	25.7	1	4.8	2	52.5
1-150-141	-1.2	-0.9	-2.1	16.8	2	3.8	2	49.2
Dapsone	-0.5	-1.3	-0.9	289.1	2		2	68.8
Trimethoprin	-1.5	-0.9	-1.2	282.8	0		3	74.3
Chloroquin	-5.3	0.4	-0,4	3718.1	3		3	100
Amodiaquine	-4.4	-0.2	0.5	1689.1	0		3	100
Mefloquine	-4;9	0.1	0.2	2903.1	0		3	100
Pamaquin	-3.8	0.4	-1.3	1475.2	0		3	100
Sulfametopyrazin	0.2	-1.7	-2.6	195.8	1		2	61.9
Tetracyclin	1.1	-2.5	-0.1	6.8	5		1	21.8
Quinacrin	-6.5	0.8	-0.7	4435.7	1		1	100
Proguanil	-1.5	-1.1	0.2	834.6	0		3	85.6
Halofantrine	-9.9	1.5	-1.4	2844.1	0		1	100
Sulfadoxine	-0.1	-1.7	-0.7	213.4	2		2	63.9
Hydroxychloroquin	-4.5	-0.1	0.2	1023.7	0		3	100
Bulaquin	-2.9	0.1	-0.4	3099.7	7		3	100
Lumefantrin	-10.01	1.7	0.2	4337.2	0		1	100
Arteether	-2.99	-0.2	0.2	5731.8	0		3	100
Dihydroartemisinin	-2.9	-0.1	-0.1	1664.9	0		3	95.4
Doxycyclin	1.7	-2.8	-2.1	9.2	4		1	20.8
Artemisinin	-2.1	-0.3	0.01	2886	1		3	95.8

[a] designed AHO analogs and known antituberculotic agents, Table 6; [b] drug likeness, number of property descriptors (24 out of the full list of 46 descriptors of QikProp, ver. 3.7, release 14) that fall outside of the range of values for 95% of known drugs; c molar mass in [g.mol^{-1}] (range for 95% of drugs: 300–500 g.mol^{-1})[37]; [d] total solvent-accessible molecular surface, in [Å^2] (probe radius 1.4 Å) (range for 95% of drugs: 300–1000 Å^2); [e] hydrophobic portion of the solvent-accessible molecular surface, in [Å^2] (probe radius 1.4 Å) (range for 95% of drugs: 0–750 Å^2); [f] total volume of molecule enclosed by solvent-accessible molecular surface, in [Å^3] (probe radius 1.4 Å) (range for 95% of drugs: 500–2000 Å^3); [g] number of non-trivial (not CX3), non-hindered (not alkene, amide, small ring) rotatable bonds (range for 95% of drugs: 0–15); [h] estimated number of hydrogen bonds that would be donated by the solute to water molecules in an aqueous solution. Values are averages taken over a number of configurations, so they can assume non-integer values (range for 95% of drugs: 0.0–6.0); [i] estimated number of hydrogen bonds that would be accepted by the solute from water molecules in an aqueous solution. Values are averages taken over a number of configurations, so they can assume non-integer values (range for 95% of drugs: 2.0–20.0); [j] logarithm of partitioning coefficient between n-octanol and water phases (range for 95% of drugs: -2 to 6.5); [k] logarithm of predicted aqueous solubility, log S in [mol.dm^{-3}] is the concentration of the solute in a saturated solution that is in equilibrium with the crystalline solid (range for 95% of drugs: -6.0 to 0.5); [l] logarithm of predicted binding constant to human serum albumin (range for 95% of drugs: -1.5 to 1.5); [m] logarithm of predicted brain/blood partition coefficient (range for 95% ofdrugs: -3.0 to 1.2); [n] predicted apparent Caco-2 cell membrane permeability in Boehringer-Ingelheim scale in [nm s-1] (range for 95% of drugs: <25 poor, >500 nm s^{-1} great); [o] number of likely metabolic reactions (range for 95% of drugs: 1–8); [p] predicted inhibition constants K_i^{pre}. K_i^{pre} was predicted from computed $\Delta\Delta G_{com}$ using the regression Equation B shown in Table 3; [q] human oral absorption (1 = low, 2 = medium, 3 = high); [r] percentage of human oral absorption in gastrointestinal tract (<25% = poor, >80% = high); * star in any columnindicates that the property descriptor value of the compound falls outside the range of values for 95% of known drugs.

DISCUSSIONS

In the search of significant improvement justifying the rise of potency from the most active training set compound AHO1 and the novel designed analogs a comparative analysis of enzyme-AHO analogs interaction energy breakdown to main *Pf*A-M1 active site residues contribution (see Figure 9). The destabilizing contribution of Arg489 in the case of AHO1 (K_i^{exp} = 27 nM) turned to stabilizing by more than 4 kcal.mol^{-1} for 1-140-141 (K_i^{pre} = 2.1nM) and 1-142-141 (K_i^{pre} = 2.3 nM) in line with the HB network (Figure 8 A: one bifurcated HB and one single HB) between 1-140-141 and the pointed residue. This interaction with Arg489 is a qualitatively stabilizing feature as reported earlier [19] but not observed for AHO1. The π - anion contact between the top 5 designed AHO analogs and Glu319 (Figure 8 B) is crucial since its kind (HB mainly)can impact negatively the N-Boc group access to the S1' pocket as reported [19]. The interaction metrics about the hydroxamic acid moiety with the catalytic triad His496, His500, and Glu519 either directly by HB or zinc ion mediated as reported [19], are kept in these new AHO analogs (Figure 9).

The top 4 best hit fit from the PH4 result were evaluated with the QSAR complexation model, equation B from table 3, in order to predict their inhibitory activity (K_i^{pre}): 1-140-141 (K_i^{pre} = 2.1nM); 1-142-141 (K_i^{pre} = 2.3 nM); 1-149-141 (K_i^{pre} = 4.8nM); 1-150-141 (K_{ipre} = 3.8nM); 1-148-141 (K_i^{pre} =4.8 nM). The pharmacophore characteristic of 1-140-141 (K_i^{pre} = 2.1nM) is displayed on figure 7.

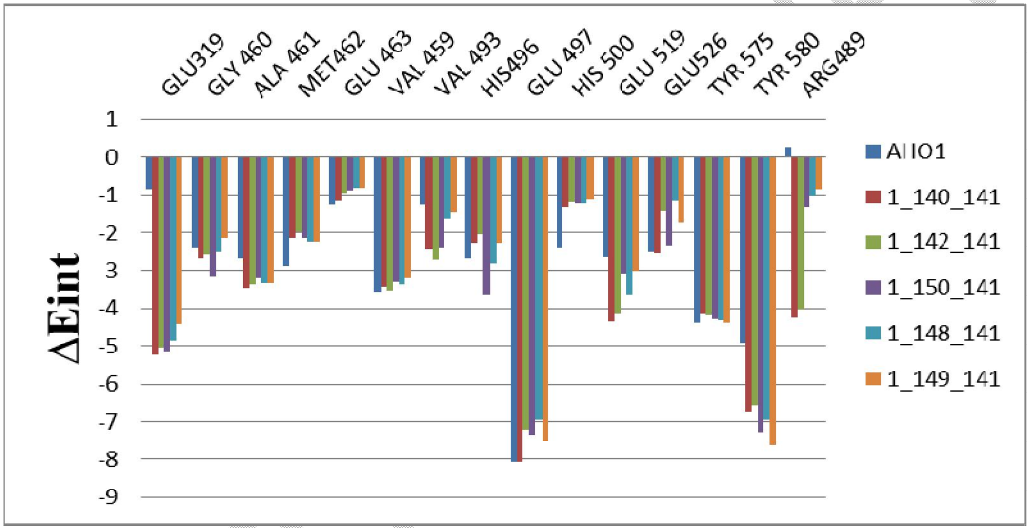

Figure9. Molecular mechanics inter-molecular interaction energy E_{int} break-down to active site residue contributions in[kcal.mol^{-1}]: the best four novel designed AHO analogs (the color coding refers to ligands given in the legend).

5. Conclusions

Reported structural information from the x-rays crystal structure of *Pf*A-M1-AHO3 complex guided the preparation of a reliable QSAR model of *Pf*A-M1 inhibitionby the hydroxamic acid inhibitors, which correlated computed Gibbs free energies of *Pf*A-M1:AHOx complex formation with observed inhibitory potencies (K_i^{exp}). Subsequently to this QSAR model, we have derived a 3D-QSAR PH4 pharmacophore model for AHO inhibitors using a training set of 17 and validation set of 3 AHOs with known inhibitory activities [19,20,21]. Visual analysis and computation of interactions between the *Pf*A-M1 and AHOs in the enzyme active-site directed us in our effort to design an initial diversity virtual combinatorial library of new AHO analogues with two substitutions on the AHO scaffold at positions R1 and R2. A resulting focused library filtered by a set of ADME-related descriptors and screened by mapping of the analogs to the PH4 pharmacophore, permitted selection of a library subset of bioavailable AHOs. The exploration of the chemical subspace keeping the AHO scaffold while R1 and R2 positions are decorated with appropriate substitutents yielded a subset of 51 best virtual hits which was submitted to computation of predicted *Pf*A-M1 inhibitory potencies by the complexation QSAR model. The best analogues reached predicted activities in the low nanomolar concentration range: 1-140-141 (K_i^{pre} = 2.1nM); 1-142-141 (K_i^{pre} = 2.3 nM); 1-149-141 (K_i^{pre} = 4.8nM); 1-150-141 (K_i^{pre} = 3.8nM); 1-

148-141 (K_i^{pre} =4.8 nM).They are recommended for synthesis and subsequent activity evaluation in *Pf*A-M1 inhibition assays and may lead to a discovery of novel potent synthetic or naturally occurring bioavailable antimalarials.

Abbreviations

2D Two-dimensional
3D Three-dimensional
ADME Absorption, distribution, metabolism, and excretion
AHO Hydroxamic acids inhibitors
AHOx Training set of Hydroxamic acids
AHOVx Validation set of Hydroxamic acids
CAMD computer-aided molecular design
E_{int} MM enzyme–inhibitor interaction energy
$\Delta\Delta G_{com}$ Relative complexation GFE
GFE Gibbs free energy
$\Delta\Delta G_{sol}$ Relative solvation GFE
HBA Hydrogen bond Acceptor
HBD Hydrogen bond Donor
H_{MM} Enthalpy component of GFE
HOA Human oral absorption
HYD Hydrophobic
HYDA Hydrophobic Aliphatic
$K_i$inhibitory concentration
IE Interaction energy
M1 metalloaminopeptidase 1
MM Molecular mechanics
MM-PB Molecular mechanics–Poisson–Boltzmann
PDB Protein Data Bank
Pf plasmodium falciparum
PfA Plasmodium falciparum aminopeptidase
PH4 Pharmacophore
QSAR Quantitative structure–activity relationships
RMSD Root-mean square deviation
SAR Structure–activity relationships
TS Training set
VS Validation set

REFERENCES

[1] *World malaria report 2021.*Geneva, World Health Organization. (2021). Licence:CC BY-NC-SA 3.0 IGO https://apps.who.int/iris/handle/10665/350147

[2] *World malaria report 2019.* Geneva: World Health Organization.(2019).Licence:CCBY-NC-SA 3.0 IGO.

[3] WorldHealth Organization (WHO), *Practical guide for treatment, severe malaria.*3rd ed.(2015) 83.

[4] A.Uwimana,E.Legrand,B.H.Stokes,J.M. Ndikumana, M. Warsame,N.Umulisa,D. Ngamije,T. Munyaneza, J.Mazarati, K.Munguti, A.M.D.Menard,Emergence and clonal expansion of in vitro artemisinin-resistant *Plasmodium falciparum kelch13* R561H mutant parasites in Rwanda, *Nat. Med.* 6 (2020)1602–1608.

[5] L.Zhu, R.W.van der Pluijm,M. Kucharski,Artemisinin resistance in the malaria parasite, Plasmodium falciparum, originates from its initial transcriptional response, *Commun. Biol. 5* (2022)274.

[6] D. Ragheb, S. Dalal, K. M. Bompiani,Distribution and biochemical properties of an M1-family aminopeptidase in Plasmodium falciparum indicate a role in vacuolar hemoglobin catabolism,*J. Biol. Chem. 286* (2011)27255–27265.

[7] S. Dalal, M. Klemba,Roles for Two Aminopeptidases in Vacuolar Hemoglobin Catabolism in Plasmodium falciparum,*J. Biol. Chem. 282* (2007)35978–35987.

[8] S. McGowan, Working in concert: the metalloaminopeptidases from *Plasmodium falciparum,Curr. Opin. Struct. Biol.*23 (2013) 828–835.

[9] A. Mucha, M. Drag, J. P. Dalton, P. Kafarski, Metallo-aminopeptidase inhibitors,*Biochimie.92* (2010) 1509–1529.

[10] E. Cunningham, *Antimicrob. Agents Chemother. 52* (2008) 3221–3228.

[11] S. McGowan, C. A. Oellig, W. A. Birru,Structure of the Plasmodium falciparum M17 aminopeptidase and significance for the design of drugs targeting the neutral exopeptidases,*Proc. Natl. Acad. Sci. USA. 107*(2010)2449–2454.

[12] K. K. Sivaraman, A. Paiardini, M. Sienczyk, C. Ruggeri, C. A. Oellig, J. P. Dalton, P. J. Scammells, M. Drag et S. McGowan, «Synthesis and structure−activity relationships of phosphonic arginine mimetics as inhibitors of the M1 and M17 aminopeptidases from *Plasmodium falciparum* », *J. Med. Chem.*56 (2013) 5213−5217.

[13] R. Verma, «Hydroxamic acids as matrix metalloproteinase inhibitors in: Gupta SP (ed) Matrix metalloproteinase inhibitors: specificity of binding and structure-activity relationships », Springer, Basel AG. 103 (2012) 137–176.

[14] G. Velmourougane, M. B. Harbut, S. Dalal,Bestatin-based chemical biology strategy reveals distinct roles for malaria M1- and M17-family aminopeptidases, *J. Med. Chem.54* (2011)1655–1666.

[15] S. McGowan, C. J. Porter, J. Lowther, C. M. Stack, S. J. Golding, T. S. Skinner-Adams, K. R. Trenholme, F. Teuscher, S. M. Donnelly, J. Grembecka, A. Mucha, P. Kafarski, R. Degori, A. M. Buckle, D. L. Gardiner, J. C. Whisstock, J.P. Dalton,Structural basis for the inhibition of the essential Plasmodium falciparum M1 neutral aminopeptidase,*Proc. Natl. Acad. Sci. U.S.A.106* (2009)2537−2542.

[16] K. Sivaraman, A. Paiardini, M. Sieńczyk, C. Ruggeri, A. Oellig, P. Dalton, J. Scammells, M. Drag et S. and McGowan,Synthesis and structure-activity relationships of phosphonic arginine mimetics as inhibitors of the M1 and M17 aminopeptidases from Plasmodium falciparum*J. Med. Chem.56* (2013)5213-5217.

[17] Graham L. Patrick, *Antimalarial Agents Design and Mechanism of Action*, Elsevier, Amsterdam, (Netherlands) 2020.

[18] R. Deprez-Poulain, M. Flipo, C. Piveteau, F. Leroux, S. Dassonneville, I. Florent, L. Maes, P. Cos, B. Deprez,Structure-activity relationships and blood distribution of antiplasmodial aminopeptidase-1 inhibitors,*J. Med. Chem.55* (2012)10909−10917.

[19] N. ShaileshMistry, N. Drinkwater, C. Ruggeri, K. K. Sivaraman, S. Logonathan , S. Fletcher, M. Drag, A. Paidini, V. M. Averg, P. J. Scaammells and M. Gowan, «Two-prongead attack: dual inhibition of *Plasmodium falciparum* M1 and M17 Metalloaminopeptidases by a new series of hydroxamic Acid-Based inhibitors », *J. Med. Chem.* 57 (2014) 9168−9183.

[20] N. Drinkwater, N.B.Vinh,D.N. Mistry,Potent dual inhibitors of *Plasmodium falciparum* M1 and M17 aminopeptidases through optimization of S1 pocket interactions, *Eur. J. Med. Chem.110 (*2016)43–64.

[21] N. B. Vinh,N.Drinkwater,T. R. Malcolm, Hydroxamic Acid Inhibitors Provide Cross-Species Inhibition of Plasmodium M1 and M17 Aminopeptidases, *J. Med. Chem. 62* (2019) 622–640.

[22] Y. Kurogi, O. F. Güner, "Pharmacophore Modeling and Three-dimensional Database Searching for Drug Design Using Catalyst," *Curr. Med. Chem.* 8 (2001) 1035-1055.

[23] Insight-II. Insight-II and Discover molecular modeling and simulation package, Version (2005). San Diego, CA: Accelrys, Inc. 2005.

[24] Discovery Studio Molecular Modeling and Simulation Program, v.2.5; Accelrys, Inc.: San Diego, CA, USA, 2009.

[25] Berman, H.M.;Westbrook, J.; Feng, Z.; Gilliland, G.; Bhat, T.N.;Weissig, H.; Shindyalov, I.N.; Bourne, P.E. The protein data bank. *Nucleic Acids Res.* (2000), 28, 235–242.

[26] K. Allangba, M. Keita, R. Kre N'Guessan, E. Megnassan, V. Frecer et S. Miertus, «Virtual design of novel *Plasmodium falciparum* cysteine protease falcipain-2 hybrid lactone chalcone and isatin-chalcone inhibitors probing the lactone chalcone and isatin-chalcone inhibitors probing the S2 active site pocket», *J. Enz. Inhib. Med. Chem.* 34 (2018) 547–561.

[27] P. Chaquin, Manual of theoretical chemistry application to structure and reactivity in molecular chemistry, pp. 190.

[28] J. Maple, M.-J. Hwang, T. Stockfisch, U. Dinur, M. Waldman, C. Ewig and A. Hagler, «Derivation of class II force fields. I. Methodology and quantum force field for the alkyl functional group and alkane molecules» *J. Comput. Chem.* 15 (1994)162–182.

[29] H. Dugas, Basic Principles in Molecular Modeling, Theoretical and Practical Aspects, 4th ed, University of Montreal Bookstore, 1996.

[30] J. Bartol, P. Comba, M. Melter and M. Zimmer, «Conformational searching of transition metal compounds», *J. Comput. Chem.* 20 (1999)1549-1558.

[31] A.F. Kouassi, M. Kone, M. Keita, A. Esmel, E. Megnassan, Y.T. N'Guessan, V. Frecer, S. Miertus. Computer-aided design of orally bioavailable pyrrolidine carboxamide inhibitors of Enoyl-Acyl Carrier Protein Reductase of *Mycobacterium tuberculosis* with favorable pharmacokinetic profiles, *Int. J. Mol. Sci.* 16 (2015) 29744–29771.

[32] Gilson, M.K.; Honig, B. The inclusion of electrostatic hydration energies in molecular mechanics calculations. *J. Comput. Aided Mol. Des.* (1991) 5, 5–20.

[33] Rocchia, W.; Sridharan, S.; Nicholls, A.; Alexov, E.; Chiabrera, A.; Honig, B. Rapid grid-based construction of the molecular surface and the use of induced surface charge to calculate reaction field energies: Applications to the molecular systems and geometric objects. *J. Comput. Chem.* (2002) 23, 128–137.

[34] Megnassan, E.; Keita, M.; Bieri, C.; Esmel, A.; Frecer, V.; Miertus, S. Design of novel dihydroxynaphthoic acid inhibitors of Plasmodium falciparum lactate dehydrogenase. *Med. Chem.* (2012) 8, 970–984.

[35] V. Frecer,S. Miertuš. Polarizable continuum model of solvation for biopolymers. *Int. J. Quantum Chem.* (1992) 42, 1449–1468.

f enoyl-acyl carrier protein reductase of Mycobacterium tuberculosis and of *Plasmodium falciparum*, *Mol .Inform.* 34 (2015) 292–307.

[36] Böttcher, C.J.F. Theory of Electric Polarization; Elsevier: Amsterdam, The

Netherlands, 1973.

[37] S. Miertuš, E. Scrocco, J. Tomasi. Electrostatic int

eraction of a solute with a continuum. A direct utilizaion of ab initio molecular potentials for the prevision of solvent effects. *Chem. Phys.* (1981) 55, 117–129.

[38] V. Frecer,S. Miertuš. Polarizable continuum model of solvation for biopolymers.

Int. J. Quantum Chem. (1992) 42, 1449–1468.

o design of phosphonic arginine and hydroxamic acid inhibitors of *Plasmodium falciparum* M17 Leucyl aminopeptidase with favorable pharmacokinetic profile », *J. Drug Des. Med. Chem.* 3 (2017) 98–125.

[40] C. A. Lipinski, F. Lombardo, B. W. Dominy, P. J. Feeney. Experimental and computational approaches to estimate solubility and permeability *in* drug discovery and development settings. *Adv Drug Deliv Rev* 46 (2001) 3–26

[41] J. Daily, «Antimalarial drug therapy: the role of parasite biology and drug resistance », *j. clin. pharmacol.* 46 (2006) 1487-1497.

[42] J. Stec, C. Vilchèze, S. Lun, A. Perryman, X. Wang, J. Freundlich et A. Kozikowski, «Biological evaluation of potent triclosan-derived inhibitors of the enoyl-acyl carrier protein reductase InhA in drug-sensitive and drug-resistant strains of *Mycobacterium tuberculosis* », *J. Med. Chem.* 9 (2014) 2528–2537.

[43] W. Jorgensen, E. Duffy, «Prediction of drug solubility from monte carlo simulations», Bioorg. Med. Chem. Lett. 10 (2000) 1155–1158.

[44] W. Jorgensen et E. Duffy, «Prediction of drug solubility from structure», Adv. Drug Delivery Rev. 54 (2002) 355–366.